Regular Article

PHYSICAL CHEMISTRY RESEARCH
Published by the
Iranian Chemical Society
www.physchemres.org
info@physchemres.org

Phys. Chem. Res., Vol. 11, No. 2, 437-447, June 2023
DOI: 10.22036/pcr.2022.336018.2070

Insights into the Electronic Properties of Coumarins: A Comparative Study Synthesis and Characterization of Fe_2O_3/Mn_2O_3 Magnetic Nanocomposites for the Photocatalytic Degradation of Methylene Blue

N.K.A. Dwijendra[a,*], I. Patra[b,*], M.J. Ansari[c], N. Saadoon[d], Z.I. Al Mashhadani[e], N.H. Obaid[f], R. Sivaraman[g], T. Alawsi[h], A.H. Jabbar[i] and Y.F. Mustafa[j]

[a]*Faculty of Engineering, Udayana University, Bali, 80361, Indonesia*

[b]*An Independent Researcher, PhD from NIT Durgapur, West Bengal, India*

[c]*Department of Pharmaceutics, College of Pharmacy, Prince Sattam Bin Abdulaziz University, Al-Kharj, Saudi Arabia*

[d]*Medical Technical College; Al-Farahidi University, Baghdad, Iraq*

[e]*Al-Nisour University College, Baghdad, Iraq*

[f]*Anesthesia Techniques Department, Al-Mustaqbal University College, Babylon, Iraq*

[g]*Department of Mathematics, Dwaraka Doss Goverdhan Doss Vaishnav College, Arumbakkam, University of Madras, Chennai, India*

[h]*Scientific Research Center, Al-Ayen University, Thi-Qar, Iraq*

[i]*Optical Department, College of Medical and Health Technology, Sawa University, Ministry of Higher Education and Scientific Research, Al-Muthanaa, Samawah, Iraq*

[j]*Department of Pharmaceutical Chemistry, College of Pharmacy, University of Mosul, Mosul-41001, Iraq*

(Received 4 April 2022, Accepted 8 July 2022)

In this paper, ferromagnetic Fe_2O_3/Mn_2O_3 nanocomposites (Fe@Mn-1 and Fe@Mn-2) were synthesized and characterized using Fourier transform infrared (FT-IR) spectroscopy, X-ray diffraction (XRD), a vibrating sample magnetometer (VSM), and transmission electron microscope (TEM). Fe@Mn-1 and Fe@Mn-2 nanocomposites were successfully synthesized and they exhibited ferromagnetic properties at room temperature and magnetic saturation of 6.48 and 9.24 emu g^{-1}, respectively. In addition, photocatalytic activities of Fe@Mn-1 and Fe@Mn-2 were studied by the degradation of methylene blue (MB) by applying H_2O_2 under visible light irradiation. The effects of important parameters on the MB degradation were evaluated, and the results exhibited the best photocatalytic activity within 45 min due to the very small crystallite sizes of Fe@Mn-1 (98%) and Fe@Mn-2 (97%).

Keywords: Photocatalysts, Nanocomposites, Degradation, Methylene blue

INTRODUCTION

Synthetic and natural organic dyes with complex aromatic structures used in different industries, such as printing, textile, paper, and pharmaceutical, are one of the major environmental pollutants in developing countries [1-11]. Due to their high stability, low bio-degradability, and production of highly toxic and carcinogenic by-products through oxidation and hydrolysis reactions in aqueous solutions, synthetic and natural organic dyes should be removed and/or degraded from aqueous solution using different techniques [1-11]. Advanced oxidation processes (AOP) using different photocatalysts were used to degrade organic dyes, such as methyl orange [12], rhodamine B [12-13], acid blue 92 [15], methylene blue [12,14,16-17], and

*Corresponding authors. E-mail: acwin@unud.ac.id; ipmagnetron0@gmail.com

reactive red 198 [18] under UV and/or visible light irradiation. In recent years, significant research has been conducted on the photodegradation of various organic dyes using Fe_2O_3- and Mn_2O_3-based nanocomposites, such as orange II [19], methyl orange [20-22], rhodamine B [22-25], acid orange 8 [26], and bisphenol A [27]. One of the viable methods proposed to improve electron transfer capabilities and prevent e^-/h^+ recombination [28] is the preparation of heterojunction metal oxide semiconductors [6-8,10,13-14,26]. For example, Xie *et al.* [14] prepared a novel heterojunction magnetic composite of $Bi_2O_3/SrFe_{12}O_{19}$ for the photo-degradation of methylene blue (MB) under visible light. Panchal *et al.* [6] reported that synthesized ZnO/MgO nanocomposites *via* plant based-green synthesis facilitated the photodegradation of MB under sunlight irradiation. Zha *et al.* [7] synthesized TiO_2/ZnO heterojunctions by the solvothermal route and reported photodegradation of methyl orange under UV light.

The aim of the present work was to synthesize Fe_2O_3/Mn_2O_3 nanocomposites using a simple and eco-friendly chemical approach in the presence of salicylic acid (Fe@Mn-1) and benzoic acid (Fe@Mn-2), accompanied by thermal decomposition at 600 °C. Moreover, the photocatalytic activity of Fe@Mn-1 and Fe@Mn-2 nanocomposites were evaluated by the degradation of MB from aqueous solution under visible light irradiation.

EXPERIMENTAL

Materials and Methods

All materials used in this study were used without further purification. FT-IR spectra were recorded on a 5DX FTIR spectrometer (Nicolet Co., USA). The X-ray diffraction (XRD) patterns were recorded using a Bruker Advance D8 diffractometer (Cu Kα radiation, λ = 1.54056 Å). The magnetic properties were investigated using a vibrating sample magnetometer with an applied magnetic field up to 14 KOe. The morphologies of samples were recorded by a transmission electron microscope (TEM, JEOL-JSM 7600 F). UV-Vis spectra were recorded in the range of 300-800 nm in a spectrophotometer (Shimadzu. UV-3600).

Synthesis of Fe_2O_3/Mn_2O_3 Nanocomposites

The α-Fe_2O_3/Mn_2O_3 nanocomposites were synthesized by a wet chemical route, accompanied by thermal decomposition at 600 °C (Scheme 1). A mixture of $FeCl_3·6H_2O$ (0.01 mmol) and $MnCl_2·4H_2O$ (0.01 mmol) was dissolved in distilled water (25 ml); then, an aqueous solution (25 ml), which contained 0.4 mmol of salicylic acid (Fe@Mn-1) and benzoic acid (Fe@Mn-2), was added to the mixture as a fuel and a surfactant. The mixture was stirred for 1.5 h at room temperature. After that, the pH of the solution was adjusted to 12 by the drop-wise addition of a 0.5 M KOH solution. The final mixture was stirred for 2 h at 75 °C. The brown precipitate was filtered, washed, dried, and calcined at 600 °C for 3 h. The resulting dark-red precipitation was collected, washed with distilled cold water, and finally dried in air for several days. Afterward, the products were characterized using FT-IR, XRD, VSM, and TEM. In addition, photocatalytic activities of Fe@Mn-1 and Fe@Mn-2 were studied by the degradation of methylene blue (MB) dye under visible light irradiation.

Photocatalytic Degradation of MB

The photocatalytic activities of Fe@Mn-1 and Fe@Mn-2 nanocomposites were studied under visible light using MB dye. In a typical experiment, a suitable quantity of Fe@Mn-1 and/or Fe@Mn-2 nanocomposites, as a

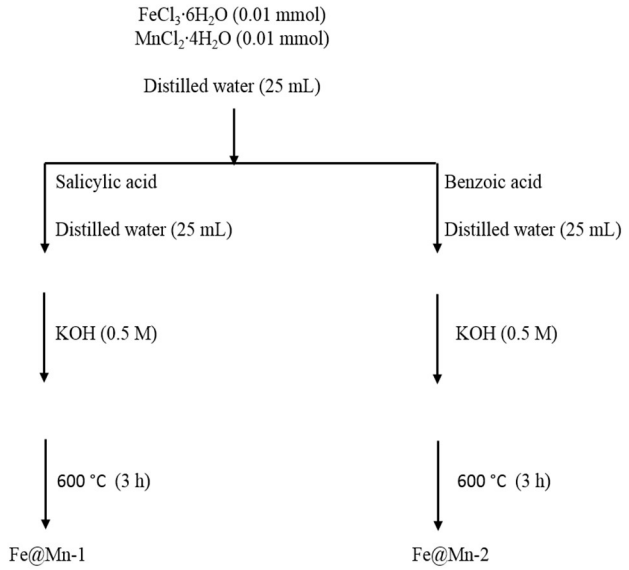

Scheme 1. The synthesis procedure of Fe@Mn-1 and Fe@Mn-2 nanocomposites.

photocatalyst, was added to a 50 ml of MB aqueous solution with an initial concentration of 30 mg l^{-1}. After that, the suspension was stirred for 30 min in the dark to achieve an adsorption/desorption equilibrium of MB molecules with the photocatalyst surface, followed by the addition of 3 ml of H_2O_2 (30%), as an electron trap, to the suspension. Then, the mixture was irradiated with 12 Philips TL 8w/54-7656 bulb lamps. After a given time interval (15, 30, 45, 60, 90, 120, and 150 min), about 4 mL of the suspension was collected, centrifuged, and analyzed by using a UV-Vis spectrophotometer and monitoring the change in the intensity of MB solution absorbance at λ_{max} of 664 nm [29-33]. The removal percentage (%) and adsorption capacity were calculated by Eq. (1), where C_o and C_t represent the initial and real-time absorbance of MB, respectively, V is the volume (l), and M is the photocatalyst dose.

$$R\ (\%) = \{(C_o - C_t) \times 100\}/C_o \quad (1)$$

$$Q\ (mg/g) = \{(C_o - C_t) \times V\}/M \quad (2)$$

RESULTS AND DISCUSSION

Characterization

FT-IR spectra of Fe@Mn-1 and/or Fe@Mn-2 nanocomposites are shown in Fig. 1. There were three adsorption bands at about 471, 534, and 608 cm^{-1} attributed to the vibrations of Fe-O and Mn-O bonds [23,26]. In addition, a very broad peak observed in both samples at about 3424 cm^{-1} can be attributed to the vibration of O-H of adsorbed water molecules [21]. As can be seen in Fig. 1, there was no difference between the FT-IR spectra of Fe@Mn-1 and/or Fe@Mn-2 nanocomposites.

The crystal phase and structure of Fe@Mn-1 and/or Fe@Mn-2 nanocomposites were investigated by XRD analysis (Figs. 2a, b). In Fig. 2, the characteristic peaks observed at 24.17 (012), 33.19 (104), 35.64 (110), 40.88 (113), 49.48 (204), 54.09 (116), 57.64 (112), 62.62 (2014), and 64.17 (300) in the XRD patterns of samples can be well assigned to the structure of hematite (α-Fe_2O_3) (JCPDS no. 33-0664) with unit-cell parameters of a = b = 5.036 Å and c = 13.749 Å [21,27] while the characteristic peaks observed at 23.16 (211), 32.98 (222), and 38.24 (400) can be assigned to the structure of braunite (α-Mn_2O_3) (JCPDS no. 89-4836)

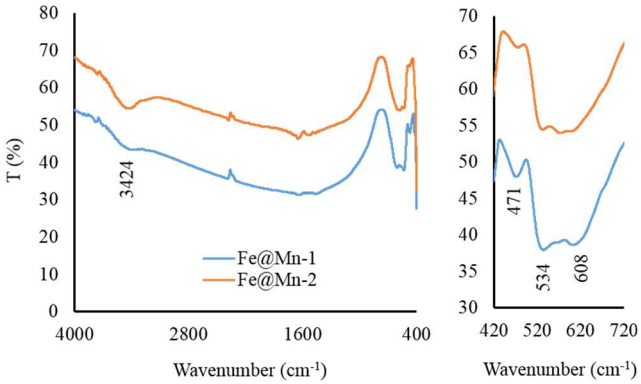

Fig. 1. FT-IR spectra of Fe@Mn-1 and Fe@Mn-2 nanocomposites.

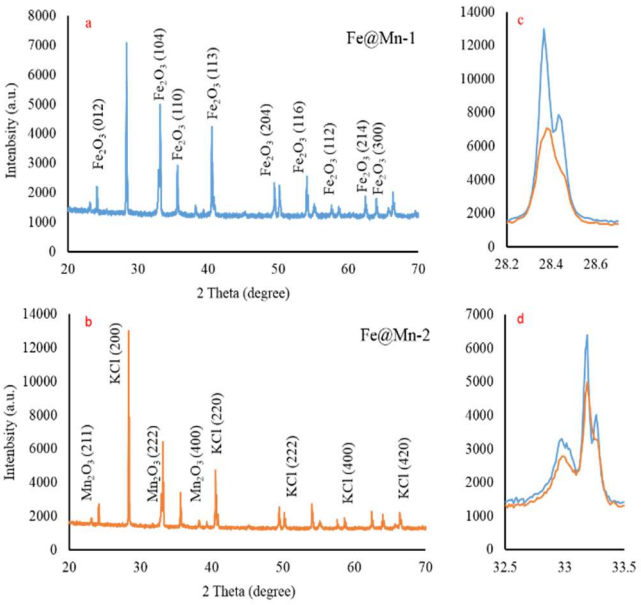

Fig. 2. The XRD patterns of Fe@Mn-1 and Fe@Mn-2 nanocomposites.

[34-36]. Finally, the characteristic peaks observed at 28.37 (200), 40.54 (220), 50.21 (222), 58.66 (400), and 66.61 (420) can be assigned to the structure of cubic KCl [37-38].

However, no difference was observed between the characteristic peaks of Fe@Mn-1 and Fe@Mn-2 nanocomposites in the XRD patterns, but the intensity of the characteristic peaks of Fe@Mn-2 was higher than that of the characteristic peaks of Fe@Mn-1, suggesting that Fe@Mn-2 had better crystallinity than Fe@Mn-1 (Figs. 2c, d). Using

the Scherrer equation (Eq. (3)), the crystallite size of the as-prepared Fe@Mn-1 and Fe@Mn-2 were calculated as 18.55 nm and 13.89 nm, respectively.

$$D\ (nm) = 0.94\lambda/\beta\cos\theta \quad (3)$$

where D is the average crystallite size (nm), λ is the wavelength (1.54 Å) of the X-ray source, β is the FWHM of the XRD peak for the (222) plane, and θ is the Bragg's angle. The magnetic hysteresis loops of Fe@Mn-1 and Fe@Mn-2 nanocomposites are illustrated in Fig. 3. The samples displayed a low coercivity (Hc) (179.5 Oe), which is characteristic of soft-magnetic materials. The saturation magnetization value obtained for Fe@Mn-1 and Fe@Mn-2 was 6.55 emu g^{-1} and 9.34 emu g^{-1}, respectively. The samples displayed apparent ferromagnetic behavior, a finding which is in good agreement with those of previous reports on α-Fe_2O_3 and Mn_2O_3 nanoparticles [39-41]. The increase in the value of M_s for Fe@Mn-2 than Fe@Mn-1 predicted that the average crystal size of Fe@Mn-2 must have been smaller than that of Fe@Mn-1 [42]. The M_s values demonstrated that the as-prepared Fe@Mn-1 and Fe@Mn-2 nanocomposites could be successfully regenerated from the solution by an external magnet [43].

TEM images of the as-synthesized Fe@Mn-1 and Fe@Mn-2 nanocomposites are shown in Fig. 4. Some small irregularly shaped nanostructures with an average crystallite size of < 20 nm are clearly observable for both samples, suggesting that the morphology and crystal size of the as-synthesized Fe@Mn-1 and Fe@Mn-2 nanocomposites depended on the precursor.

The absorbance spectra and Tauc plot of Fe@Mn-1 and Fe@Mn-2 nanocomposites are represented in Fig. 5. There were two broad peaks at about 440 and 560 nm [44-46]. The direct optical band gap of Fe@Mn-1 and Fe@Mn-2 nanocomposites was calculated to be 2.73 and 2.27 eV using the Tauc equation (Eq. (5)) [45-46], where α is the Kubelka-Munk function, K is constant, and E_g is the band gap energy.

$$(\alpha h\upsilon)^2 = B\ (h\upsilon - E_g) \quad (5)$$

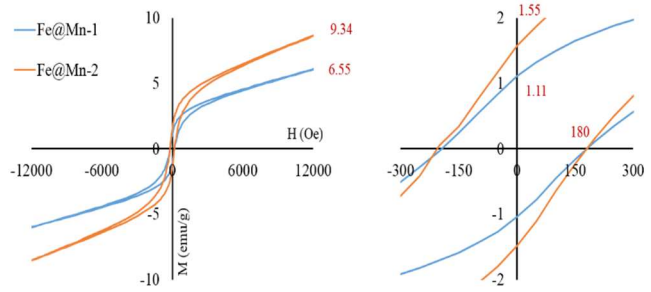

Fig. 3. The magnetic hysteresis loops of Fe@Mn-1 and Fe@Mn-2 nanocomposites.

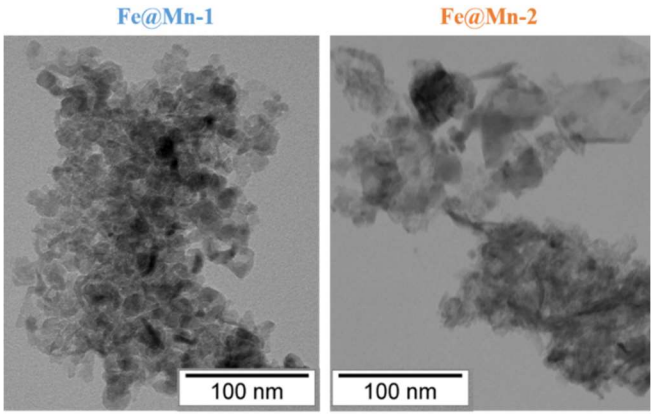

Fig. 4. The TEM images of Fe@Mn-1 and Fe@Mn-2 nanocomposites.

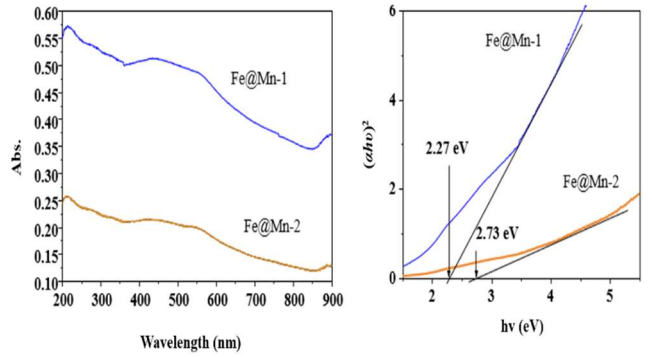

Fig. 5. Absorbance spectra and Tauc plot of Fe@Mn-1 and Fe@Mn-2 nanocomposites.

MB Photodegradation Studies

Until now, the photocatalytic activities of different catalysts have been evaluated by the degradation of MB aqueous solution under UV and/or visible light irradiation [6,14,17,47-55]. Also, the effects of various parameters, such as catalyst dosage, time irradiation, and initial MB

concentration, have been investigated by the photodegradation of MB. Due to its impact on the surface charge of catalysts, the pH solution affects organic dye photodegradation and is thus considered an important parameter in the photocatalytic process [56]. Due to the presence of the OH group on the surface of transition metal oxides [25], their surface charge depended on the pH solution. As shown in Fig. 6, the point of zero charge (PZC) of Fe@Mn-1 and/or Fe@Mn-2 was almost equal (6.45 and 6.63). According to zeta analysis, Fe@Mn-1 and Fe@Mn also had similar isoelectric points. When the pH solution was < 6.7 due to the formation of $FeOH_2^+$ groups, the surface charge of Fe@Mn-1 and Fe@Mn-2 became positive. Therefore, the repulsion between the positive charge of MB and the surface of the photocatalyst reduced the photodegradation efficiency of MB dye [25]. However, at pH > 6.7, the surface charge of samples became negative due to the formation of FeO^-, leading to increased photodegradation efficiency. Figure 7 shows the effect of pH solution on the photodegradation of MB at pH values in the range of 3-11. As can be seen in Fig. 7, the photodegradation of MB in acidic solutions was very low [56]. Degradation efficiency increased with increasing pH (97% and 99% at pH = 11). The maximum adsorption capacity for Fe@Mn-1 and Fe@Mn-2 was calculated as 72.75 and 74.25 mg/g, respectively, at the optimum condition (pH 11 and 0.02 g photocatalyst). Given that the negative charge on the surface of catalysts increases increasing pH, it was expected that the adsorption of MB, as a cationic dye, on the surface of Fe@Mn-1 and/or Fe@Mn-2 nanocomposites would increase at higher pH values [57-58]. Therefore, to investigate time irradiation and photocatalyst dosage, the pH of the solution was adjusted to 11.

The effect of initial photocatalyst dosage and visible light irradiation time on the photodegradation of MB was investigated using various dosages (0.005, 0.01, 0.02, and 0.03 g) of the Fe@Mn-1 and/or Fe@Mn-2 in 30 ml of MB dye solution (30 mg l^{-1}) from 0 to 150 min, and the results are shown in Fig. 8. As can be seen in Fig. 6, when the amount of photocatalyst was increased from 0.005 to 0.03 g, the dye removal efficiency was found to be increasing, which could have been caused by an increased number of active sites on the catalyst surface. Furthermore, the results indicated that the photocatalytic activity of Fe@Mn-1 and Fe@Mn-2

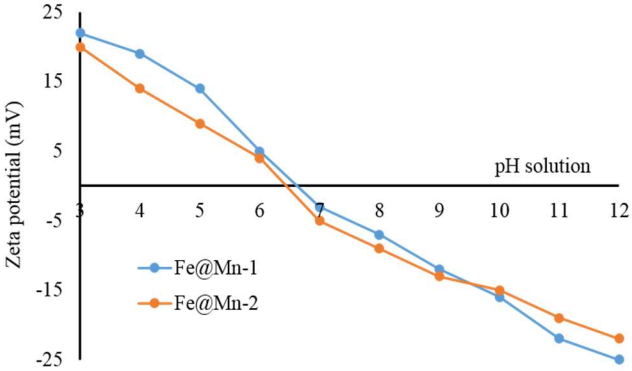

Fig. 6. Zeta potential of Fe@Mn-1 and Fe@Mn-2 nanocomposites measured in aqueous solution of MB solutions.

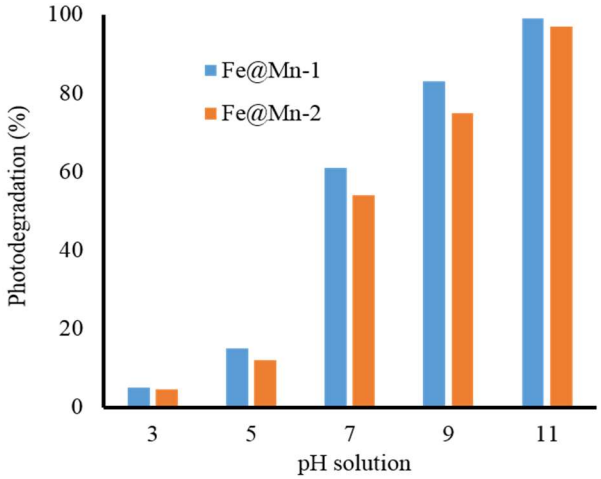

Fig. 7. The effect of the pH of the solution on the photodegradation (%) of MB (30 mg l^{-1}) (120 min visible light irradiation and 0.02 g photocatalyst).

completely degraded MB after about 90 and 120 min of irradiation time [30,59-61].

The pseudo-first-order kinetic model (Eq. (4)) has been widely applied for the photocatalytic degradation of organic dyes, such as methyl orange [22,43], rhodamine B [23,25,62], bisphenol A [27], and MB [6,29,49,61,63,64] using different photocatalysts.

$$\ln(C/C_o) = -k_1 t \quad (4)$$

where k_1 is the reaction rate constant.

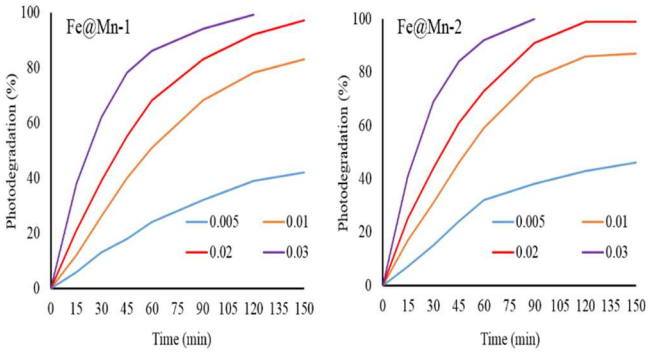

Fig. 8. The effect of irradiation time and catalyst dosage of Fe@Mn-1 and Fe@Mn-2 on MB photodegradation.

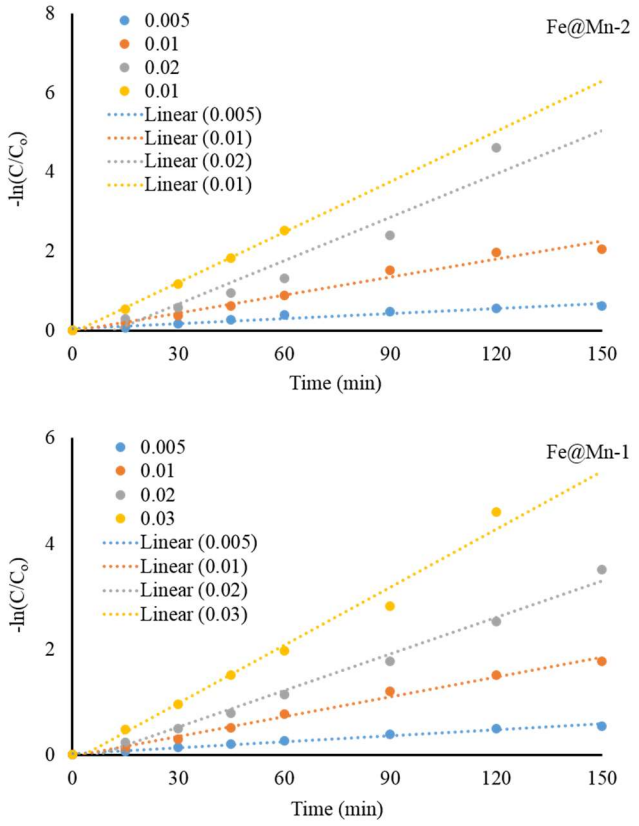

Fig. 9. The pseudo-first-order kinetic model of MB degradation.

As can be seen in Fig. 9, the photodegradation of MB using as-prepared samples followed a first-order rate low. The rate constant k_1 increased with the increases in the photocatalyst dosage from 0.0036 to 0.0384 min^{-1} for Fe@Mn-1 and from 0.0041 to 0.0421 min^{-1} for Fe@Mn-2.

The efficiency of the photocatalytic degradation of MB using as-prepared Fe@Mn-1 and Fe@Mn-1 nanocomposites was compared with that of other photocatalysts (Table 1), and the results demonstrated the superiority of the as-prepared nanocomposites.

The possible degradation mechanism of MB using Fe@Mn-1 and Fe@Mn-2 is explained in Eqs. ((5)-(10)) [25,30,59-61]:

$$Fe@Mn + h\nu \rightarrow h^{+}_{VB} + e^{-}_{CB} \quad (5)$$

$$e^{-}_{CB} + O_2 \rightarrow O_2^{-\circ} \quad (6)$$

$$H_2O_2 + e^{-}_{CB} \rightarrow OH^{\circ} + OH^{-} \quad (7)$$

$$O_2^{-\circ} + H_2O \rightarrow HO_2^{\circ} + OH^{-} \quad (8)$$

$$HO_2^{\circ} + H_2O \rightarrow OH^{\circ} + H_2O_2 \quad (9)$$

$$MB/MO + OH^{\circ} \rightarrow \text{Degraded products} \quad (10)$$

Table 1. A Comparison of MB Photodegradation with Different Photocatalysts

Photocatalyst	Degradation efficiency (%)	Irradiation time (min)	Ref.
ZnO/MgO nanocomposites	89.5	120	[6]
α-Fe_2O_3 fibers	66	300	[29]
α-Fe_2O_3 nanoparticles	96	90	[45]
Coral-like Fe_2O_3 nanoparticles	95	75	[46]
CeO_2 nanofibers	98	60	[63]
CeO_2	99	70	[65]
Fe_3O_4@SiO_2@CeO_2	92	50	[66]
Pristine CeO2 nanostructure	100	175	[67]
$MgFe_2O_4$	87	120	[68]

CONCLUSIONS

In this work, Fe_2O_3/Mn_2O_3 nanocomposites (Fe@Mn-1 and Fe@Mn-2) were synthesized through a wet chemical route and characterized using FT-IR, XRD, VSM, and TEM. The VSM results confirmed that the Fe@Mn-1 and Fe@Mn-2 nanocomposites had ferromagnetic properties at room temperature with a magnetic saturation of 6.48 and 9.24 emu g^{-1}, respectively. The photocatalytic activities of Fe@Mn-1 and Fe@Mn-2 nanocomposites can be improved by applying H_2O_2, as an electron trap, under visible light irradiation. The photocatalytic results showed 97% and 99% photodegradation efficiency for Fe@Mn-1 and Fe@Mn-2, respectively.

ACKNOWLEDGMENTS

M. J. Ansari would like to acknowledge the support of the Deanship of Scientific Research at Prince Sattam bin Abdulaziz University, Al-Kharj, Saudi Arabia.

REFERENCES

[1] Gao, S.; Zhang, W.; Zhou, H.; Chen, D., Magnetic composite Fe_3O_4/CeO_2 for adsorption of azo dye, *J. Rare Earths* **2018**, *36*, 986-993. DOI: 10.1016/j.jre.2018.04.002.

[2] Sarvari, H.; Ghoharshadi, E. K.; Samiee, S.; Ashraf, N., Removal of methyl orange from aqueous solutions by ferromagnetic Fe/Ni nanoparticles, *Phys. Chem. Res.* **2018**, *6*, 433-446. DOI: 10.22036/pcr.2018.108928.1437.

[3] YasiniArdakani, S. S.; Abghari, R.; Mirjalili, M., TiO_2@$CoFe_2O_4$ nanofiber for the photocatalytic degradation of Direct Red 80, *Phys. Chem. Res.* **2019**, *7*, 309-325. DOI: 10.22036/pcr.2019.158459.1567.

[4] Hamzehloo, M.; Farahani, B. K. A.; Rostamian, R., Adsorption behavior of reactive black dye 5 by magnetically separable nano-adsorbent, *Phys. Chem. Res.* **2019**, *7*, 475-490. DOI: 10.22036/pcr.2019.186198.1639.

[5] Heddi, D.; Benkhaled, A.; Boussaid, A.; Choukchou-Braham, E., Adsorption of anionic dyes on poly(N-vinylpyrrolidone) modified bentonite, *Phys. Chem. Res.* **2019**, *7*, 731-749. DOI: 10.22036/pcr.2019.179510.1625.

[6] Panchal, P.; Paul, D. R.; Sharma, A.; Hooda, D.; Yadav, R.; Meena, P.; Nehra, S. P., Phytoextract mediated ZnO/MgO nanocomposites for photocatalytic and antibacterial activities, *J. Photochem. Photobiol. A: Chem.* **2019**, *385*, 112049. DOI: 10.1016/j.jphotochem.2019.112049.

[7] Zha, R.; Nadimicherla, R.; Guo, X., Ultraviolet photocatalytic degradation of methyl orange by nanostructured TiO_2/ZnO heterojunctions, *J. Mater. Chem. A* **2015**, *3*, 6565-6574. DOI: 10.1039/c5ta00764j.

[8] Karamipour, A.; Rasouli, N.; Movahedi, M.; Salavati, H., A kinetic study on adsorption of congo red from aqueous solution by ZnO-$ZnFe_2O_4$-polypyrrole magnetic nanocomposite, *Phys. Chem. Res.* **2016**, *4*, 291-301. DOI: 10.22036/pcr.2016.14114.

[9] Akbartabar, I.; Yazdanshenas, M. E.; Tayebi, H. A.; Nasirzadeh, N., Physical chemistry studies of acid dye removal from aqueous media by mesoporous nano composite: Adsorption isotherm, kinetic and thermodynamic studies, *Phys. Chem. Res.* **2017**, *5*, 659-679. DOI: 10.22036/pcr.2017.83378.1371.

[10] Issarapanacheewin, S.; Wetchakun, K.; Phanichphant, S.; Kangwansupamonkon, W.; Wetchakun, N., Efficient photocatalytic degradation of rhodamine B by a novel CeO_2/Bi_2WO_6 composite film, *Catal. Today* **2016**, *278*, 280-290. DOI: 10.1016/j.cattod.2015.12.028.

[11] Qi, G.; Hai, C.; SShen, Y.; Zeng, J.; Li, X.; Ren, X.; Sun, Y.; Dong, S.; Zhou, Y., Synthesis of mono-dispersed mesoporous Mn_2O_3 powders with micro-nanostructure for removing congo red dye from aqueous solution, *Adv. Powder Technol*. **2019**, *30*, 930-939. DOI: 10.1016/j.apt.2019.02.007.

[12] Heidari, A.; Moghimi, H.; Rashidiani, J.; Taheri, R. A., Molecular development of silver nanoparticles-loaded poly acrylic acid hydrogel as a catalyst for dye degradation, *Phys. Chem. Res.* **2018**, *6*, 857-869. DOI: 10.22036/pcr.2018.145269.1528.

[13] Habibi-Yangjeh, A.; Golzad-Nonakaran, B., Fabrication of magnetically recoverable nanocomposites by combination of Fe_3O_4/ZnO with AgI and Ag_2CO_3: Substantially enhanced photocatalytic activity under visible light, *Phys. Chem. Res.* **2018**, *6*, 415-431. DOI: 10.22036/pcr.2018.116937.1461.

[14] Xie, T.; Liu, C.; Xu, L.; Yang, J.; Zhou, W., Novel heterojunction $Bi_2O_3/SrFe_{12}O_{19}$ magnetic photocatalyst

with highly enhanced photocatalytic activity, *J. Phys. Chem. C.* **2013**, *117*, 24601-24610. DOI: 10.1021/jp408627e.

[15] Salari, H.; Daliri, A.; Gholami, M. R., Graphitic carbon nitride/reduced graphene oxide/silver oxide nanostructures with enhanced photocatalytic activity in visible light, *Phys. Chem. Res.* **2018**, *6*, 729-740. DOI: 10.22036/pcr.2018.137083.1501.

[16] Abbasi, Z.; Farrokhnia, A.; Garcia-Lopez, E.I.; ZargarShoushtari, M., Codeposition of Fe_3O_4 nanoparticles sandwiched between g-C_3N_4 and TiO_2nanosheets: Structure, characterization and high photocatalytic activity for efficiently degradation of dye pollutants, *Phys. Chem. Res.* **2019**, *7*, 65-80. DOI: 10.22036/pcr.2019.147945.1537.

[17] Sahu, K.; Singh, J.; Mohapatra, S., Photocatalytic and catalytic removal of toxic pollutants from water using CuOnanosheets, *J. Mater. Sci: Mater. Electron.* **2019**, *30*, 6088-6099. DOI: 10.1007/s10854.019-00910-3.

[18] Mahmood, N. M., Zinc ferrite nanoparticles as a magnetic catalyst: Synthesis and dye degradation, *Mater. Res. Bull.* **2013**, *48*, 4255-4260. DOI: 10.1016/j.materresbull.2013.06.070.

[19] Jiang, T.; Poyraz, A. S.; Iyer, A.; Zhang, Y.; Luo, Z.; Zhong, W.; Miao, R.; El-Sawy, A. M.; Guild, C. J.; Sun, Y.; Kriz, D. A.; Suib, S. L., Synthesis of mesoporous iron oxides by an inverse micelle method and their application in the degradation of orange II under visible light and natural pH, *J. Phys. Chem. C* **2015**, *119*, 10454-10468. DOI: 10.1021/acs-jpcc.5b02057.

[20] Munusamy, G.; Mani, R.; Varadharajan, K.; Narasimhan, S.; Munusamy, C.; Chandrasekaran, B., α-Fe_2O_3@carbon core-shell nanostructure for luminescent upconversion and photocatalytic degradation of methyl orange, *Res. Chem. Intermed.* **2020**, *46*, 715-736. DOI: 10.1007/s11164-019-03986-y.

[21] Khalaji, A. D; Machek, P.; Jarosova, M., α-Fe_2O_3 nanoparticles: Synthesis, characterization, magnetic properties and photocatalytic degradation of methyl orange, *Adv. J. Chem. A* **2021**, *4*, 317-326. DOI: 10.22034/AJCA-2016-1268.

[22] Gandha, K.; Mohapatra, J.; Hossain, M. K.; Elkins, K.; Poudyal, N.; Rajeshwar, K.; Liu, J. P., Mesoporous iron oxide nanowires: synthesis, magnetic and photocatalytic properties, *RSC Adv*. **2016**, *6*, 90537-90546. DOI: 10.1039/C6RA18530D.

[23] Qiu, M.; Wang, R.; Qi, X., Hollow polyhedral α-Fe_2O_3 prepared by self-assembly and its photocatalytic activities in degradation of RhB, *J. Taiwan Inst. Chem. Eng.* **2019**, *102*, 394-402. DOI: 10.1016/j.jtice.2019.05.024.

[24] Liu, X.; Chen, K.; Shim, J. J.; Huang, J., Facile synthesis of porous Fe_2O_3nanorods and their photocatalytic properties, *J. Saudi Chem. Soc*. **2015**, *19*, 479-484. DOI: 10.1016/j.jscd.2015.06.009.

[25] Kusior, A.; Michalec, K.; Jelen, P.; Radecka, M., Shaped Fe_2O_3 nanoparticles-synthesis and enhanced photocatalytic degradation towards RhB, *App. Surf. Sci.* **2019**, *476*, 342-352. DOI: 10.1016/j.apsusc.2018.12.113.

[26] Abebe, B.; Zereffa, E. A.; Ananda Murthy, H. C., Synthesis of poly(vinyl alcohol)-aided ZnO/Mn_2O_3 nanocomposites for acid orange-8 dye degradation, mechanism and antibacterial activity, *ACS Omega* **2021**, *6*, 954-964. DOI: 10.1021/acsomega.0c05597.

[27] Ye, C.; Hu, K.; Niu, Z.; Lu, Y.; Zhang, L.; Yan, K., Controllable synthesis of rhombohedral α-Fe_2O_3 efficient for photocatalytic degradation of bisphenol A, *J. Water Process Eng.* **2019**, *27*, 205-210. DOI: 10.1016/j.jwpe.2018.12.008.

[28] Mohd Adnan, M. A.; Julkapli, N. M.; Abd Hamid, S. B., Review on ZnO hybrid photocatalysts: Impact on photocatalytic activities of water pollutant degradation, *Rev. Inorg. Chem*. **2016**, *36*, 77-104. DOI: 10.1515/revic-2015-0015.

[29]Araujo, R. N.; Nascimento, E. P.; Firmino, H.C.T.; Macedo, D. A. Neves, G. A.; Morales, M. A.; Menezes, R. R., α-Fe_2O_3 fibers: An efficient photocatalyst for dye degradation under visible light, *J. All. Comp.* **2021***, 882*, 160683. DOI: 10.1016/j.jallcom.2021.160683.

[30] Lassoued, A.; Lassoued, M. S.; Dkhil, B.; Ammar, S.; Gadri, A., Nanocrystalline$Ni_xCo_{(0.5-x)}Zn_{0.5}Fe_2O_4$ ferrite: fabrication through co-precipitation route with enhanced structural, magnetic and photocatalytic activity. *J. Mater. Sci.: Mater. Electron*. **2018**, *29*, 7333-7344. DOI: 10.1007/s10854-018-8723-y.

[31] Jasim, S. A.; Machek, P.; Abdelbasset, W. K.; Jarosova, M.; Majdi, H. S.; Khalaji. S. A., Solution combustion

synthesis of CeO_2 nanoparticles for excellent photocatalytic degradation of methylene blue, *Appl. Phys. A* **2022**, *128*, 475. DOI: 10.1007/s00339-022-05532-x.

[32] Hakimi, M.; Morvaridi, M.; Hosseini, H.A.; Alimard, P., Preparation, characterization and photocatalytic activity of Bi_2O_3-Al_2O_3 nanocomposite, *Polyhedron* **2019**, *170*, 523-529. DOI: 10.1016/j.poly.2019.06.029.

[33] Saadoon, S. J.; Jarosova, M.; Machek, P.; Kadhim, M. M.; Ali, M. H.; Khalaji, A. D., Methylene blue photodegradation using as-synthesized CeO_2 nanoparticles, *J. Chin. Chem. Soc.* **2021**, *69*, 280-288. DOI: 10.1002/jccs.202100476.

[34] Liang, C.; Wang, H.; Huang, K.; Lin, S.; Liu, W.; Bi, K.; Lei, M., Hierarchically porous $MgMn_2O_4$ microspheres assembled with nanosheets as high oxygen reduction catalyst, *Catal. Lett.* **2019**, *149*, 1903-1910. DOI: 10.1007/s10562-019-02760-4.

[35] Najjar, R.; Awad, R.; Abdel-Gaber, A. M., Physical properties of Mn_2O_3 nanoparticles synthesized by co-precipitation method at different pH values, *J.Superconduc. Novel Mag.* **2019**, *32*, 885-892. DOI: 10.1007/s10948-018-4765-x.

[36] Hanifehpour, Y.; Cheney, M. A.; Joo, S. W., Sonocatalyticdecolorization of azo dye by ultrasound-assisted ytterbium-substituted Mn_2O_3 nanocatalyst, *J. Inorg. Organomet. Polym. Mater.* **2019**, *28*, 2143-2153. DOI: 10.1007/s10904-018-0881-0.

[37] Agarwal, M.; Garg, S. K.; Asokan, K.; Kanjilal, D.; Kumar, P., Facile synthesis of KCl:Sm^{3+} nanophosphor as a new OSL dosimetric material achieved through charge transfer between the defect states, *RSC Adv*. **2017**, *7*, 13836-13845.DOI: 10.1039/c6ra25237k.

[38] Ismail, S. N.; Ali, E. M.; Alwan, B. J.; Abd, A. N., Potassium chloride canoparticles: cynthesis, characterization, and study the antimicrobial applications, *Macromol. Symp.* **2022**, *401*, 2100312. DOI: 10.1002/masy.202100312.

[39] Mazrouaa, A. M.; Mohamed, M. G.; Fekry, M., Physical and magnetic properties of iron oxide nanoparticles with a different molar ratio of ferrous and ferric, *Egypt. J. Petrol*. **2019**, *28*, 165-171. DOI: 10.1016/j.ejpe.219.02.002.

[40] Talebi, R., New method for preparation Mn_2O_3-TiO_2 nanocomposites and study of their photocatalytic properties, *J. Mater. Sci: Mater. Electron.* **2017**, *28*, 8316-8321. DOI: 10.1007/s10854-017-6546-x.

[41] Huang, Y.; Nengzi, L. C.; Zhang, X.; Gou, J.; Gao, Y.; Zhu, G.; Cheng, Q.; Cheng, X., Catalytic degradation of ciprofloxacin by magnetic CuS/Fe_2O_3/Mn_2O_3 nanocomposite activated peroxymonosulfate: Influence factors, degradation pathways and reaction mechanism, *Chem. Eng. J.* **2020**, *388*, 124274. DOI: 10.1016/j.cej.2020.124274.

[42] Lassoued, A.; Lassoued, M. S.; Dkhil, B.; Ammar, S.; Gadri, A., Synthesis, photoluminescence and magnetic properties of iron oxide (α-F_2O_3) nanoparticles through precipitation or hydrothermal methods, *Physica E* **2018**, *10*, 212-219. DOI: 10.1016/j.physe.2018.04.009.

[43] Wang, J.; Saho, X.; Zhang, X.; Tian, G.; Ji, X.; Bao, W., Preparation of mesoporous magnetic Fe_2O_3 nanoparticle and its application for organic dyes removal, *J. Mol. Liq*. **2017**, *248*, 13-18. DOI: 10.1016/j.molliq.2017.10.026.

[44] Khalaji, A. D., Spherical α-Fe_2O_3 nanoparticle: Synthesis and characterization and its photocatalytic degradation of methyl orange and methylene blue, *Phys. Chem. Res.* **2022**, *10*, 473-483.

[45] KassegnWeldegebrieal, G.; KassegnSibhatu, A., Photocatalytic activity of biosynthesized α-Fe_2O_3 nanoparticles for the degradation of methylene blue and methyl orange dyes, *Optik*, **2021**, *241*, 167226. DOI: 10.1016/j.ijleo.2021.167226.

[46] Gupta, N. K.; Ghaffari, Y.; Bae, J.; Kim, K. S., Synthesis of coral-like α-Fe_2O_3 nanoparticles for dye degradation at neutral pH, *J. Mol. Liq*. **2020**, *301*, 112473. DOI: 10.1016/j.molliq.2020.112473.

[47] Paul, D. R.; Sharma, R.; Nehra, S. P.; Sharma, A., Effect of calcination temperature, pH and catalyst loading on photodegradation efficiency of urea derived graphitic carbon nitride towards methylene blue dye solution, *RSC Adv*. **2019**, *9*, 15381-15391. DOI: 10.1039/c9ra02201e.

[48] Neena, D.; Kondamareddy, K. K.; Bin, H.; Lu, D.; Kumar, P.; Dwivedi, R. K.; Pelenovich, V. O.; Zhao, X. Z.; Gao, W.; Fu, D., Enhanced visible light photodegradation activity of RhB/MB from aqueous

solution using nanosized novel Fe-Cd co-modified ZnO, *Sci. Rep.* **2018**, *8*, 10691. DOI: 10.1038/s41598-018-29025-1.

[49] Kamarudin, N. S.; Jusoh, R.; Setiabudi, H. D.; Sukor, N. F., Photodegradation of methylene blue using phyto-mediated synthesis of silver nanoparticles: effect of calcination treatment, *Mater. Today: Proceed*. **2018**, *5*, 21981-21989. DOI: 10.1016/j.matpr.2018.07.059.

[50] Ghaffari, Y.; Kumar Gupta, N.; Bae, J.; Soo Kim K., One-step fabrication of Fe_2O_3/Mn_2O_3 nanocomposite for rapid photodegradation of organic dyes at neutral pH, *J. Mol. Liq*. **2020**, *315*, 113691. DOI: 10.1016/j.molliq.2020.113691.

[51] Fang, J.; Xu, J.; Chen, J.; Huang, X.; Wang, X., Enhanced photocatalytic activity of molecular imprinted nano α-Fe_2O_3 by hydrothermal synthesis using methylene blue as structure-directing agent, *Coll. Surf. A: Physicochem. Eng. Aspects* **2016**, *508*, 124-134. DOI: 10.1016/j.colsurfa.2016.08.048.

[52] da Nóbrega Silva, E.; OuriquesBrasileiro, I. L.; Stumpf Madeira, V.; Aranhade Farias, B.; Almeida Ramalho, M. L.; Rodríguez-Aguado, E.; Rodríguez-Castellón, E., Reusable $CuFe_2O_4$-Fe_2O_3 catalyst synthesis and application for the heterogeneous photo-Fenton degradation of methylene blue in visible light, *J. Environ. Chem. Eng*. **2020**, *8*, 104132. DOI: 10.1016/j.jece.2020.104132.

[53] Norouzi, A.; Nezamzadeh-Ejhieh, A., α-Fe_2O_3/Cu_2O heterostructure: Brief characterization and kinetic aspect of degradation of methylene blue, *Phys. B: Cond. Matter.* **2020**, *599*, 412422. DOI: 10.1016/j.physb.2020.412422.

[54] Norouzi, A.; Nezamzadeh-Ejhieh, A., Preparation, characterization, and investigation of the catalytic property of α-Fe_2O_3-ZnO nanoparticles in the photodegradation and mineralization of methylene blue, *Chem. Phys. Lett.* **2020**, *752*, 137587. DOI: 10.1016/j.cplett.2020.137587.

[55]Phuruangrat, A.; Kuntalue, B.; Thongtem, S.; Thongtem, T., Hydrothermal synthesis of hexagonal ZnOnanoplates used for photodegradation of methylene blue, *Optik*, **2021**, *226*, 165949. DOI: 10.1016/j.ijleo.2020.165949.

[56] Abdellah, M. H.; Nosier, S. A.; El-Shazl, A. H.; Mubarak, A. A., Photocatalytic decolorization of methylene blue using TiO_2/UV system enhanced by air sparging. *Alex. Eng. J.* **2018**, *57*, 3727-3735. DOI: 10.1016/j.aej.2018.07.018.

[57] Liu, Y.; Yu, H.; Lv, Z.; Zhan, S.; Yang, J.; Peng, X.; Ren, Y.; Wu, X., Simulated-sunlight-activated photocatalysis of Methylene Blue using cerium doped SiO_2/TiO_2 nanostructured fibers. *J. Environ. Sci.* **2012**, *24*, 1867-1875. DOI: 10.1016/S1001-0742(11)61008-5.

[58] Jing, H. P.; Wang, C. C.; Zhang, Y. W.; Wang, P.; Li, R., Photocatalytic degradation of methylene blue in ZIF-8. *RSC Adv.* **2014**, *4*, 54454. DOI: 10.1039/C4RA08820D.

[59] Lassoued, A.; Lassoued, M. S.; Dkhil, B.; Ammar, S.; Gadri, A., Photocatalytic degradation of methyl orange dye by $NiFe_2O_4$ nanoparticles under visible irradiation: effect of varying the synthesis temperature. *J. Mater. Sci: Mater. Electron*. **2018**, *29*, 7057-7067. DOI: 10.1007/s10854-018-8693-0.

[60] Snthilkumar, S.; Lellala, K.; Ashok, M.; Priyadharsan, A.; Sanjeeviraja, C.; Rajendran, A., Green synthesis of CeO_2-TiO_2 compound using clomechelidonii leaf extract foexceleentphotocatalytic acticity. *J. Mater. Sci.: Mater. Electron*. **2018**, *29*, 14023-14030. DOI: 10.1007/s10854-018-9534-x.

[61] Vatanparast, M.; Saedi, L., Sonochemical-assisted synthesis and characterization of CeO_2 nanoparticles and its photocatalytic properties. *J. Mater. Sci: Mater. Electron*. **2018**, *29*, 7107-7113. DOI: 10.1007/s10854-018-8698-8.

[62] Anna Becker, K. K.; Bloesser, A.; Weller, T. Timm, J.; Suchomski, C.; Marschall, E., Stabilization of monodisperse, phase-pure $MgFe_2O_4$ nanoparticles in aqueous and nonaqueous media and their photocatalytic behavior, *J. Phys. Chem. C* **2017**, *121*, 2712-27138. DOI: 10.1021/acs.lpcc.7b08780.

[63] Ynag, X.; Liu, Y.; Li, J.; Zhang, Y., Effect of calcination temperature on morphology and structure of CeO_2 nanofibers and their photocatalytic activity, *Mater. Lett*. **2019**, *241*, 76-79. DOI: 10.1016/j.matlet.2019.01.006

[64]Salari, H.; Yaghmaei, H., Z-scheme 3D Bi_2WO_6/MnO_2 heterojunction for increased photoinduced charge separation and enhanced Abdellah, M. H.; Nosier, S. A.; El-Shazl, A. H.;

X147413. DOI: 10.1016/j.apsusc.2020.147413.

[65] Safat, S.; Buazar, F.; Albukhaty, S.; Matroodi, S., Enhanced sunlight photocatalytic activity and biosafety of marine-driven synthesized cerium oxide nanoparticles, *Sci. Rep*. **2021**, *11*, 14734. DOI: 10.1038/s41597-021-94327-w.

[66] Ziaadini F.; Mostafavi, A.; Shamspur, T.; Fathirad, F., Photocatalytic degradation of methylene blue from aqueous solution using De_3O_4@SiO_2@CeO_2 core-shell magnetic nanostructure as an effective catalyst, DOI: 10.22104/AET.2020.4137.1204.

Adv. Environ. Technol. **2019**, *2*, 127-132.

[67] Majumder, D.; Chakraborty, I.; Mandal, K.; Roy, S., Facet-dependent photodegradation of methylene blue using pristine CeO2 nanostructures, *ACS Omega* **2019**, *4*, 4243-4251. DOI: 10.1021/acsomega.8b03298.

[68] Hammache, Z.; Soukeur, A.; Omeiri, S.; Bellal, B.; Trari, M., Physical and photo-electrochemical properties of $MgFe_2O_4$ prepared by sol gel route: application to the photodegradation of methylene blue, *J. Mater. Sci: Mater Electron.* **2019**, *30*, 5375-5382. DOI: 10.1007/s10854-019-00830-2.